

A crossover in phase diagram of $\text{NaFe}_{1-x}\text{Co}_x\text{As}$ determined by electronic transport measurements

A. F. Wang, J. J. Ying, X. G. Luo, Y. J. Yan, Z. J. Xiang, P. Cheng, G. J. Ye, and X. H. Chen*
*Hefei National Laboratory for Physical Science at Microscale and Department of Physics,
 University of Science and Technology of China, Hefei, Anhui 230026, People's Republic of China*

D. Y. Liu and L. J. Zou
*Key Laboratory of Materials Physics, Institute of Solid State Physics,
 Chinese Academy of Sciences, P. O. Box 1129, Hefei 230031, People's Republic of China*

Z. Sun

National Synchrotron Radiation Laboratory, University of Science and Technology of China, Hefei, Anhui 230029, People's Republic of China

We report electronic transport measurements on single crystals of $\text{NaFe}_{1-x}\text{Co}_x\text{As}$ system. We found that the cotangent of Hall angle, $\cot\theta_H$, follows T^4 for the parent compound with filamentary superconductivity and T^2 for the heavily-overdoped non-superconducting sample. While it exhibits approximately T^3 -dependence in all the superconducting samples, suggesting this behavior is associated with bulk superconductivity in ferropnictides. A deviation develops below a characteristic temperature T^* well above the structural and superconducting transitions, accompanied by a departure from power-law temperature dependence in resistivity. The doping dependence of T^* resembles the crossover line of pseudogap phase in cuprates.

PACS numbers: 74.62.-c; 74.25.F-; 74.70.Xa

I. INTRODUCTION

The ferropnictide and cuprate high-temperature superconductors share some key similarities - an antiferromagnetism in parent compounds, the quasi-two-dimensional nature of superconducting CuO_2 and FeAs layers¹⁻⁴, and the emerging superconductivity realized by suppressing the antiferromagnetic ground states^{5,6}. A natural question is whether the two families have the same mechanism for superconductivity. In cuprate compounds, the nature of pseudogap phase is a key issue in understanding the high-temperature superconductivity. The evidence from resistivity⁷, Nernst effect⁸, inelastic neutron scattering⁹⁻¹¹ and scanning tunnelling spectroscopy^{12,13} indicated that the pseudogap phase in cuprates is an electronic state that breaks rotational symmetry of underlying lattice with stripe or nematic order. Compared with the phase diagram of cuprates, the current interest in ferropnictides lies in the peculiar normal-state properties of these materials to detect whether there exists a pseudogap-like state.

In ferropnictides, the electronic nematicity has been detected by in-plane resistivity anisotropy¹⁴, angle-resolved photoemission measurements¹⁵, scanning tunnelling spectroscopy¹⁶ and inelastic neutron scattering¹⁷. In these studies, the structural distortions that break the crystal's C_4 rotational symmetry may apply external driving forces to induce the electronic nematicity. Very recently, magnetic torque measurements by Kasahara *et al.* revealed a nematic transition at high temperatures above the structural and superconducting transitions in $\text{BaFe}_2(\text{As}_{1-x}\text{P}_x)_2$, with a characteristic temperature similar to the pseudogap crossover in cuprate superconductors¹⁸. Without the potential external driving forces from the lattice, this transition can be

considered to be induced by the electronic system only.

However, there lacks evidence directly related to the electronic properties of the high-temperature nematic transition reported by Kasahara *et al.*. For an evident phase transition, such as the superconducting, antiferromagnetic and structural transitions in ferropnictides, specific heat data show anomalies at corresponding temperatures. It becomes nontrivial to locate the crossover line and determine the phase diagram. In this letter, we study the resistivity and Hall coefficient measurements on high-quality single crystals of $\text{NaFe}_{1-x}\text{Co}_x\text{As}$. At high temperatures, the Hall angle, $\cot\theta_H$, reveals T^3 -dependence for superconducting samples. Below a crossover temperature T^* , the resistivity and Hall angle deviate from power-law temperature dependence. In the electronic phase diagram, T^* depicts a characteristic temperature similar to the pseudogap crossover in cuprate superconductors.

II. EXPERIMENTAL DETAILS

High-quality single crystals of $\text{NaFe}_{1-x}\text{Co}_x\text{As}$ were grown by the NaAs flux method¹⁹. The accurate chemical composition of the single crystals was determined by energy dispersive X-ray spectroscopy (EDS). The standard instrument error for this method is around 10%. The single crystals of $x = 0, 0.010, 0.014, 0.017, 0.028, 0.042, 0.047, 0.061, 0.075$ and 0.109 were measured, with a high quality characterized and demonstrated in our previous report¹⁹. X-ray diffraction (XRD) was performed on Smartlab-9 diffractometer (Rikagu) from 10° to 60° with a scanning rate of $2^\circ/\text{minute}$. Measurements of resistivity and Hall effect were conducted by using the PPMS-9T (Quantum Design). The resistivity were measured using the standard four-probe method. The contacts cover the sides of the samples to ensure in-plane transport. Hall coefficient was measured by sweeping the field from -5T to 5T at various temperatures. We firstly confirmed the linear-

*Corresponding author; Electronic address: chenxh@ustc.edu.cn

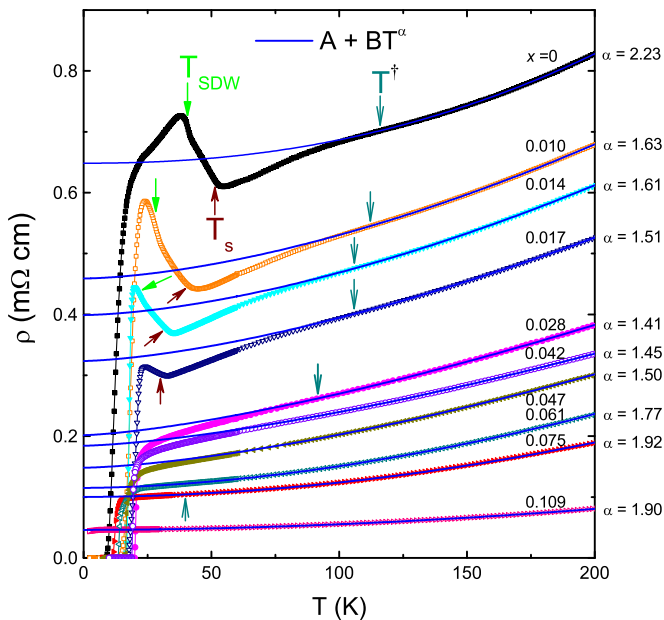


FIG. 1: Temperature dependence of in-plane resistivity for $\text{NaFe}_{1-x}\text{Co}_x\text{As}$ single crystals. The solid line is the fitting curve by power-law temperature dependence with the formula: $\rho = A + B \times T^\alpha$ to the resistivity data. The power-law exponents, α , are shown on the right of the panel, which decrease from 2.23 for $x = 0$ to 1.41 for the optimal doping level and then increase to 1.90 for the heavily overdoped sample. Obvious deviation from the high-temperature power-law behavior can be seen in resistivity and the deviation temperature (T^\dagger) decreases with increasing Co concentration. In addition, the characteristic temperatures of SDW and structural transitions are also marked as T_{SDW} and T_s .

ity of Hall resistivity ρ_{xy} to magnetic field in the normal state. An excellent linearity can be observed for all the samples in the normal state except that a very weak deviation from the linearity appears below T_{SDW} in underdoped samples. Then the temperature dependence of Hall coefficients was obtained from the subtraction of the voltages measured at 5 T and -5 T, $R_H = [V_{xy}(5T) - V_{xy}(-5T)] \times d/2I$, where d is the thickness of crystals and I is the current. The cotangent of Hall angle, $\cot\theta_H = \rho/\rho_{xy}$, was calculated at 5 T, where ρ_{xy} is Hall resistivity. It should be addressed that the Hall coefficient can not be well measured at the temperature above 200 K, the possible reason is that Na ions could move above 200 K. All the samples we used are the same with that in our previous work¹⁹ and the T_c , T_{SDW} and T_s are summarized in Table 1 and plotted in Fig. 6. All the superconducting samples show nearly full shielding fraction except for the parent compound with filamentary superconductivity.

III. RESULTS AND DISCUSSION

We carefully measured the resistivity on single crystals of $\text{NaFe}_{1-x}\text{Co}_x\text{As}$ system with $x = 0 - 0.109$ ranging from the parent compound to the heavily overdoped non-superconducting composition as shown in Fig. 1. For the

parent compound and the underdoped crystals, there exists an upturn in resistivity below 50 K due to the structural and spin density wave (SDW) transitions¹⁹. An evident feature is that the resistivity curvature changes well above the T_s in parent compound and all underdoped samples. For the optimally doped and overdoped crystals, there seems no anomaly in the normal-state resistivity. In the high-temperature cuprate superconductors, the mapping of in-plane resistivity curvature is a useful way to determine electronic phase diagrams. In particular, the pseudogap crossover line can be conveniently obtained by this method²⁰. Here, we made power law fitting on the resistivity data with formula $\rho = A + B \times T^\alpha$ and show them in Fig.1. One can see that the resistivity follows power-law dependence at high temperature and starts to deviate at a characteristic temperature, T^\dagger , for all the samples. The doping dependence of T^\dagger will be shown in Fig. 6. For the heavily overdoped non-superconducting sample ($x = 0.109$), no deviation from the power-law dependence can be observed. As shown in Fig. 1, the power-law exponent α decreases with increasing Co doping from the parent compound to the optimally doped crystals, and then increases with Co concentration in the overdoped region. The α reaches the smallest value of 1.41 in the optimally doped sample.

To accurately determine the T^\dagger , we plot $(\rho - A)/T^\alpha$ vs. temperature, as shown in Fig. 2. The characteristic temperature T^\dagger can be well defined, at which ρ starts to deviate from the power-law temperature dependence. As shown in Fig. 2, the heavily overdoped crystal with $x=0.109$ shows a deviation from the power-law temperature dependence due to a tiny superconducting transition around 6 K, so that we take the $T^\dagger=0$ K. The deviation temperature, T^\dagger , determined by our fitting is highly repeatable. Table 1 summarizes the T^\dagger , which monotonically decreases with increasing Co concentration and goes to zero in the heavily overdoped non-superconducting compound ($x = 0.109$). We should address that the variation of the temperature region used for fitting does not change the deviation temperature T^\dagger , significantly, which suggests that our results are reliable.

Figure 3 shows the temperature dependence of Hall coefficients, R_H , for various single crystals of $\text{NaFe}_{1-x}\text{Co}_x\text{As}$. The Hall coefficients show a systematic evolution with increasing Co doping with a strong temperature dependence. The magnitude of Hall coefficients at room temperature increases upon Co doping, and then sharply decreases for the heavily overdoped non-superconducting sample with a value smaller than those of superconducting samples. It is worth noting that the Hall coefficient in the non-superconducting $x = 0.109$ compound is nearly independent of temperature, bearing a feature that is usually found in a conventional Fermi-liquid metal. This behavior suggests that $\text{NaFe}_{1-x}\text{Co}_x\text{As}$ becomes a traditional metallic material at very high doping levels. The abrupt increase below 50 K in magnitude of Hall coefficients for the underdoped samples is due to the structural transition.

The complicated properties of temperature dependent Hall coefficients can be expressed in a simple fashion by looking at the cotangent of Hall angle: $\cot\theta_H = \rho/\rho_{xy}$ ²¹ as shown in Fig. 4, where ρ_{xy} is Hall resistivity. It is interesting to notice that $\cot\theta_H$ shows power-law temperature dependence for all

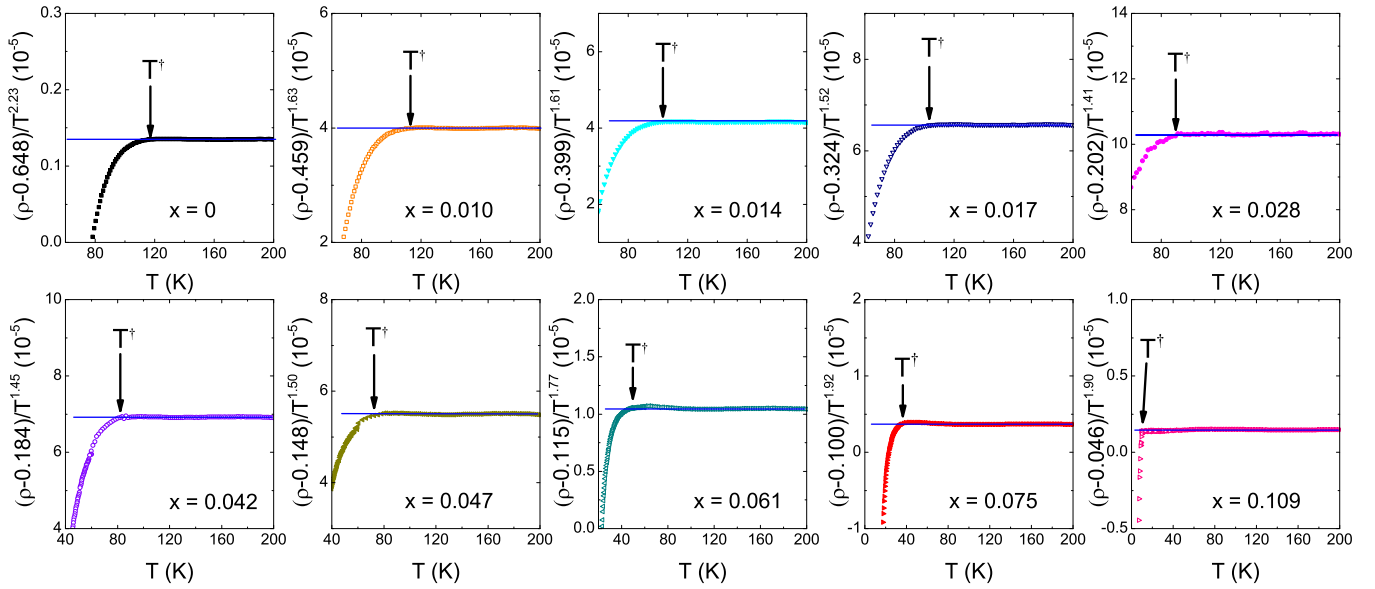


FIG. 2: $(\rho - A)/T^\alpha$ as a function of temperature for all the crystals of $\text{NaFe}_{1-x}\text{Co}_x\text{As}$. It clearly shows the temperature at which the deviation from the high-temperature power-law dependence of in-plane resistivity ρ . The dashed lines guide eyes for the the $A+B \times T^\alpha$ dependence. The deviation at T^\dagger is marked by arrows.

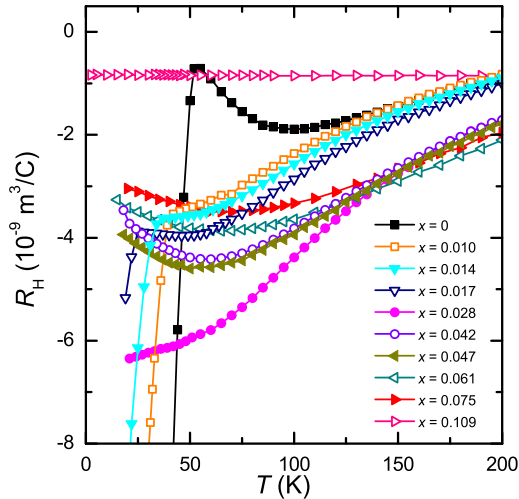


FIG. 3: Temperature dependence of Hall coefficient, R_H , for various single crystals of $\text{NaFe}_{1-x}\text{Co}_x\text{As}$.

the single crystals of $\text{NaFe}_{1-x}\text{Co}_x\text{As}$: T^4 for the parent compound, approximately T^3 for all the superconducting crystals, and T^2 for the heavily-overdoped non-superconducting sample. T^β -dependent $\cot\theta_H$ with $\beta=2.5 \sim 3.0$ has been reported in $\text{BaFe}_{2-x}\text{Co}_x\text{As}_2$ single crystals²². In cuprates, $\cot\theta_H$ behaves approximately as $T^{2.1}$, regardless of materials and doping level, except that T^4 -dependence is found in the electron-doped cuprates²³, which is interpreted by the multi-band ef-

fect with different contributions from various bands.

A careful examination on Fig. 4 indicates slight curvatures in the plot, suggesting that the best power-laws in a wide temperature range deviate slightly from an integer β . Fig. 5 shows plots of $(\cot\theta_H - C)/T^\beta$ vs. T for all the samples, in which the power-law temperature dependence is canceled out, so that one can easily see the temperature range in which the T^β behavior holds well. Here, C is the offset value and β is the best power. In Fig. 5, the power-law temperature dependent $\cot\theta_H$ holds very well down to a characteristic temperature, T^* , for all the samples. Below T^* , $\cot\theta_H$ departs from the power-law (T^β) behavior. This characteristic temperature decreases with increasing Co doping and goes to zero in the heavily overdoped non-superconducting sample. One may notice that the deviation goes in different directions for various doping, which is probably related to the details in the quasiparticle scattering processes that varies with Co concentrations. We should address that the variation of the temperature region used for fitting does not change the deviation temperature T^* , significantly, which suggests that our results are reliable.

Fig. 6 shows the phase diagram and we plot T^\dagger and T^* as a function of doping. The two characteristic temperatures are highly consistent with each other, though they are obtained by different methods. Generally, both T^\dagger and T^* decreases with increasing Co doping, and goes to zero at the doping level $x = 0.109$ where T_c goes to zero. The phase diagram in Fig. 6 is quite similar to the pseudogap phase diagram of the high-temperature cuprate superconductors. Indeed, the deviation of $\cot\theta_H$ from T^2 dependence has been used to characterize the onset of pseudogap in hole-doped cuprate superconductors²⁴, and the pseudogap crossover line can be conveniently determined by resistivity curvature mapping²⁰. Here, these methods were used to determine the T^\dagger and T^* and reveal the

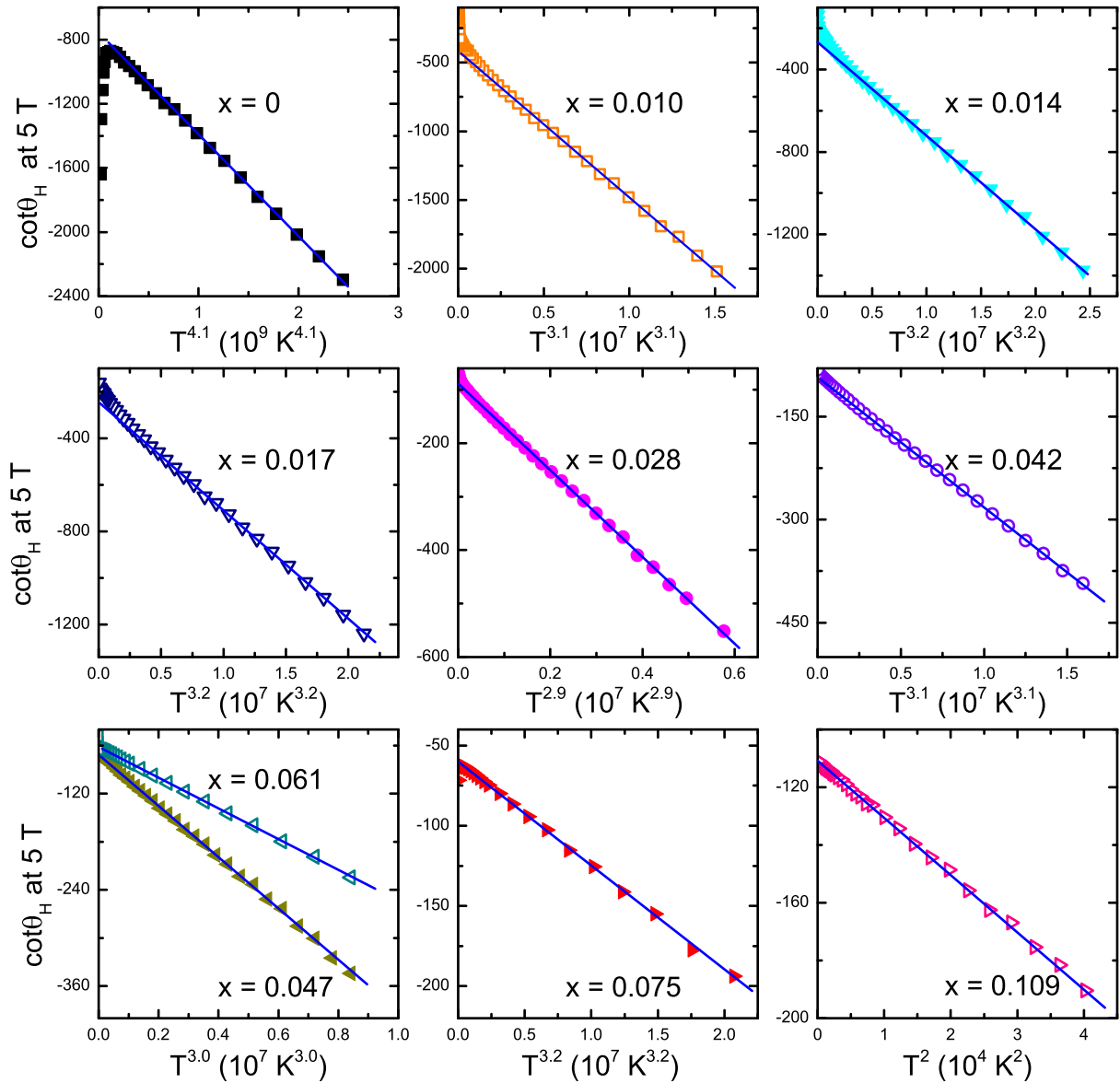


FIG. 4: The $\cot\theta_H$ plotted in power-law temperature scale for $\text{NaFe}_{1-x}\text{Co}_x\text{As}$ single crystals. All the superconducting samples show approximately T^3 dependent $\cot\theta_H$ except for the parent compound with filamentary superconductivity.

crossover line above the structural and superconducting transitions. Our data strongly suggests that a crossover occurs at the T^* in ferropnictide superconductors. We are cautious that our data do not indicate any "gapping" behavior as observed in cuprates, though we stress the similarity between characteristic T^* temperature and the pseudogap crossover temperature

A natural question is what happens below the T^* . Without the driving forces from structural or magnetic transitions, the T^* indicates a crossover with purely electronic origin. A possible scenario is that the electronic nematic state sets in below the characteristic temperature. Indeed, a similar crossover induced by electronic nematicity has been observed in $\text{BaFe}_2(\text{As}_{1-x}\text{P}_x)_2$ well above the structural and superconducting transitions¹⁸. The Hall angle exhibits approximate T^3 -dependence for all the superconducting crystals, while the

parent compound with filamentary superconductivity and the heavily overdoped non-superconducting crystal exhibit a different behavior. This finding suggests that the T^3 -dependence of $\cot\theta_H$ is tied to the superconducting regime.

IV. CONCLUSION

In conclusion, Our electronic transport studies reveal the existence of a crossover temperature well above structural and magnetic transitions. In the phase diagram of $\text{NaFe}_{1-x}\text{Co}_x\text{As}$, the crossover line resembles the pseudogap phase diagram in cuprate superconductors. An interesting phenomenon is that the Hall angle reveals approximate T^3 -dependence of $\cot\theta_H$ in the whole superconducting regime, suggesting this

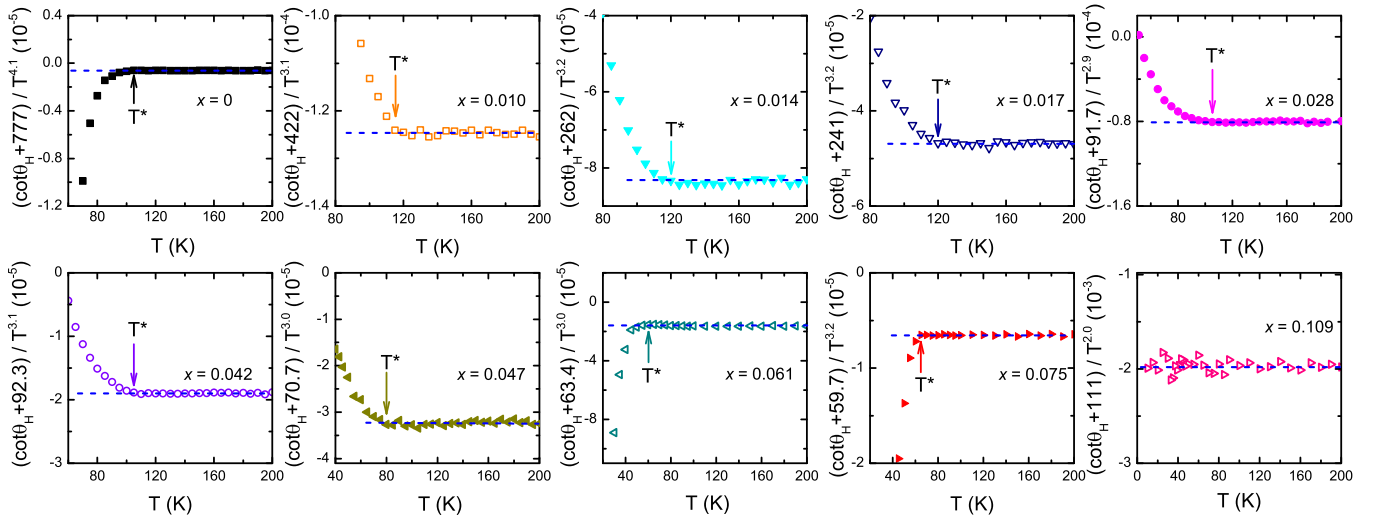


FIG. 5: $(\cot\theta_H - C)/T^\beta$ as a function of temperature for all the crystals of $\text{NaFe}_{1-x}\text{Co}_x\text{As}$. It clearly shows the temperature at which the deviation from the high-temperature power-law dependent $\cot\theta_H$. The dashed lines guide eyes for the the $C+D\times T^\beta$ dependence. The deviation at T^* is marked by arrows.

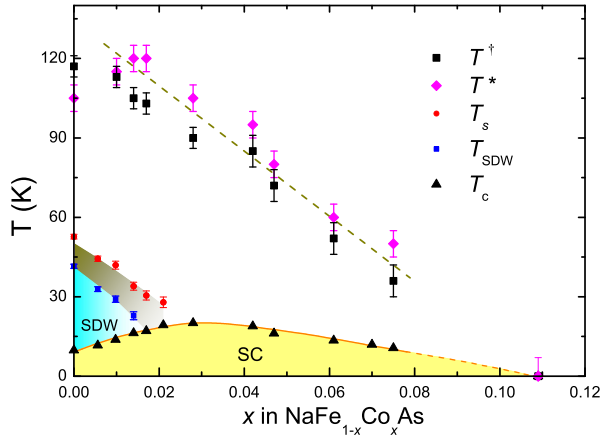


FIG. 6: Phase diagram of $\text{NaFe}_{1-x}\text{Co}_x\text{As}$ system. The superconducting transition temperature, T_c , spin density wave (SDW) transition temperature, T_{SDW} , and structural transition temperature, T_s , and structural transition temperature, T_s , were determined from resistivity, susceptibility and specific heat measurements by our group¹⁹. For the parent compound, the specific heat shows the structural and SDW transitions with no anomaly at T_c , suggesting a filamentary superconductivity. T^\dagger and T^* were determined in Figs. 2 and Fig. 5, respectively.

behavior is associated with bulk superconductivity in ferropnictides. These findings shed light on the mechanism of the high-temperature superconductivity in ferropnictides and potentially the superconductivity in cuprates as well.

ACKNOWLEDGEMENTS X.H. Chen would like to thank Yayu Wang, Zheng-Yu Weng and J. P. Hu for stimulating discussion and suggestion. This work is supported by National Natural Science Foundation of China (Grant No. 11190021, 51021091), the National Basic Research Program of China (973 Program, Grant No. 2012CB922002 and No. 2011CBA00101), and Chinese Academy of Sciences.

- ¹ Y. Kamihara, T. Watanabe, M. Hirano, and H. Hosono, *J. Am. Chem. Soc.* **130**, 3296(2008).
- ² X. H. Chen, T. Wu, G. Wu, R. H. Liu, H. Chen and D. F. Fang, *Nature* **453**, 761(2008).
- ³ Clarina de la Cruz, Q. Huang, J. W. Lynn, Jiying Li, W. Ratcliff II, J. L. Zarestky, H. A. Mook, G. F. Chen, J. L. Luo, N. L. Wang and Pengcheng Dai, *Nature* **453**, 899 (2008).
- ⁴ Athena S. Sefat, Rongying Jin, Michael A. McGuire, Brian C. Sales, David J. Singh, and David Mandrus, *Phys. Rev. Lett.* **101**, 117004 (2008).

- ⁵ P.A. Lee, N. Nagaosa and X.G. Wen, *Rev. Mod. Phys.* **78**,17(2006).
- ⁶ J. Paglione and R.L. Greene, *Nature Phys.* **6**, 645(2010).
- ⁷ Yoichi Ando, Kouji Segawa, Seiki Komiya, and A. N. Lavrov, *Phys. Rev. Lett.* **88**, 137005(2002).
- ⁸ R. Daou, J. Chang, David Leboeuf, Olivier Cyr-Choinire, Francis Lalibert, Nicolas Doiron-Leyraud, B. J. Ramshaw, Ruixing Liang, D. A. Bonn, W. N. Hardy, Louis Taillefer, *Nature* **463**, 519(2010).
- ⁹ C. Stock, W. J. L. Buyers, R. Liang, D. Peets, Z. Tun, D. Bonn, W. N. Hardy, and R. J. Birgeneau, *Phys. Rev. B* **69**, 014502(2004).

TABLE I: The temperatures plotted in the phase diagram (see Fig. 6 in the manuscript).

x	T_c (K)	T_{SDW} (K)	T_s (K)	T^* (K)	T^\dagger (K)
0	9.8 ± 0.3	40.6 ± 1.0	51.4 ± 1.0	105 ± 5	116 ± 4
0.010	13.8 ± 0.3	28.2 ± 1.0	41.0 ± 1.5	115 ± 5	113 ± 4
0.014	16.3 ± 0.3	21.8 ± 1.5	32.1 ± 1.5	120 ± 5	106 ± 4
0.017	17.1 ± 0.3		30.0 ± 1.8	120 ± 5	103 ± 4
0.028	20.1 ± 0.3			105 ± 5	92 ± 4
0.042	18.9 ± 0.3			95 ± 5	85 ± 6
0.047	16.2 ± 0.3			80 ± 5	70 ± 6
0.061	13.5 ± 0.3			60 ± 5	52 ± 6
0.075	10.7 ± 0.3			50 ± 5	40 ± 6
0.109	0			0	0

- ¹⁰ V. Hinkov, P. Bourges, S. Pailhs, Y. Sidis, A. Ivanov, C. D. Frost, T. G. Perring, C. T. Lin, D. P. Chen and B. Keimer, *Nature Phys.* **3**, 780(2007).
- ¹¹ V. Hinkov, D. Haug, B. Fauqu, P. Bourges, Y. Sidis, A. Ivanov, C. Bernhard, C. T. Lin and B. Keimer, *Science* **319**, 597(2008).
- ¹² Y. Kohsaka, C. Taylor, K. Fujita, A. Schmidt, C. Lupien, T. Hanaguri, M. Azuma, M. Takano, H. Eisaki, H. Takagi, S. Uchida and J. C. Davis, *Science* **315**, 1380(2007).
- ¹³ Y. Kohsaka, C. Taylor, P. Wahl, A. Schmidt, Jhinhwan Lee, K. Fujita, J. W. Alldredge, K. McElroy, Jinho Lee, H. Eisaki, S. Uchida, D.-H. Lee and J. C. Davis, *Nature* **454**, 1072(2007).
- ¹⁴ Jiun-Haw Chu, James G. Analytis, Kristiaan De Greve, Peter L.

- McMahon, Zahirul Islam, Yoshihisa Yamamoto, Ian R. Fisher, *Science* **329**, 824(2010).
- ¹⁵ M. Yi, D. Lu, J.-H. Chu, J. G. Analytis, A. P. Sorini, A. F. Kemper, B. Moritz, S.-K. Mo, R. G. Moore, M. Hashimoto, W.-S. Lee, Z. Hussain, T. P. Devereaux, I. R. Fisher, and Z.-X. Shen, *Proc. Natl. Acad. Sci. USA* **108**, 6878(2011).
- ¹⁶ T.-M. Chuang, M. P. Allan, Jinho Lee, Yang Xie, Ni Ni, S. L. Budko, G. S. Boebinger, P. C. Canfield, J. C. Davis, *Science* **327**, 181(2010).
- ¹⁷ Jun Zhao, D. T. Adroja, Dao-Xin Yao, R. Bewley, Shiliang Li, X. F. Wang, G. Wu, X. H. Chen, Jiangping Hu and Pengcheng Dai, *Nature Phys.* **5**, 555(2009).
- ¹⁸ S. Kasahara, H. J. Shi, K. Hashimoto, S. Tonegawa, Y. Mizukami, T. Shibauchi, K. Sugimoto, T. Fukuda, T. Terashima, Andriy H. Nevidomskyy and Y. Matsuda, *Nature* **486**, 382(2012).
- ¹⁹ A. F. Wang, X. G. Luo, Y. J. Yan, J. J. Ying, Z. J. Xiang, G. J. Ye, P. Cheng, Z. Y. Li, W. J. Hu, and X. H. Chen, *Phys. Rev. B* **85**, 224521(2012).
- ²⁰ Yoichi Ando, Seiki Komiya, Kouji Segawa, S. Ono, and Y. Kurita, *Phys. Rev. Lett.* **93**, 267001(2004).
- ²¹ T.R. Chien, Z.Z. Wang and N.P. Ong, *Phys. Rev. Lett.* **67**, 2088(1991).
- ²² E. Arushanov, S. Levchenko, G. Fuchs, B. Holzapfel, S. L. Drechsler, L. Schultz, *J. Supercond. Nov. Magn.* **24**, 2285(2011).
- ²³ C. H. Wang, G. Y. Wang, T. Wu, Z. Feng, X. G. Luo, and X. H. Chen, *Phys. Rev. B* **72**, 132506(2005); Y. Dagan and R.L. Greene, *Phys. Rev. B* **76**, 024506(2007).
- ²⁴ Y. Abe, K. Segawa and Y. Ando, *Phys. Rev. B* **60**, 15055(R)(1999).